

Phosphine-Based Z-Selective Ruthenium Olefin Metathesis Catalysts

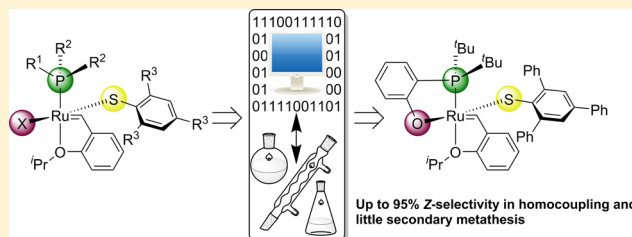
Wietse Smit, Vitali Koudriavtsev, Giovanni Occhipinti,* Karl W. Törnroos, and Vidar R. Jensen*

Department of Chemistry, University of Bergen, Allégaten 41, N-5007 Bergen, Norway

Supporting Information

ABSTRACT: Whereas a number of highly Z-selective ruthenium-based olefin metathesis catalysts bearing N-heterocyclic carbene ligands have been reported in recent years, Z-selectivity has so far been difficult to achieve for phosphine-based catalysts. Guided by predictive density functional theory (DFT) calculations, we have developed phosphine-based ruthenium olefin metathesis catalysts giving 70–95% of the Z-isomer product in homocoupling of terminal alkenes such as allylbenzene, 1-octene, allyl acetate, and 2-allyloxyethanol.

Starting from a moderately selective catalyst, $[P(\text{Cy})_3](-S-2,4,6\text{-Ph-C}_6\text{H}_2)\text{ClRu}(\text{=CH-O}^i\text{PrC}_6\text{H}_4)$ (**4**, Cy = cyclohexyl, ⁱPr = isopropyl), obtained by substituting a chloride of the Hoveyda–Grubbs first-generation catalyst with 2,4,6-triphenylbenzenethiolate, we moved on to replace Cl and PCy₃ by chelating, anionic phosphine ligands. Such ligands increase selectivity by limiting rotation around the P–Ru bond and by specifically directing the steric bulk of the phosphine substituents toward the selectivity-inducing thiolate ligand. In particular, DFT calculations predicted that *o*-(dialkylphosphino)phenolate ligands should improve selectivity and activity compared to **4**. The most promising of these compounds (**8b**), based on the *o*-(di-*tert*-butylphosphino)phenolate ligand, directs the two P-bonded *tert*-butyl substituents toward the 2,4,6-triphenylbenzenethiolate and has little steric hindrance *trans* to the thiolate. This compound metathesizes terminal olefins such as allylbenzene and 1-octene with Z-selectivities above 80% and allylacetate above 90%. Although these phosphine-based ruthenium monothiolate catalysts in general achieve somewhat lower activities and Z-selectivities than their second-generation counterparts, they also offer examples giving less substrate and product isomerization and thus higher yields.



INTRODUCTION

Olefin metathesis is an important carbon–carbon coupling method of the organic chemist’s toolbox. It is, for instance, used extensively in the synthesis of natural products^{1–3} and polymers^{4,5} and in oleochemistry⁶ and has found applications even in peptide and protein modifications.^{7–10} Metathesis of terminal olefins to give disubstituted olefins typically results in mixtures of the Z- and E-isomers, with the thermodynamically more stable E-isomer usually being the major product. Separating these isomers is costly and often challenging, which may hamper the assessment of their activity and the application of olefin metathesis in medicinal chemistry.^{11–13}

In recent years, several catalysts with enhanced Z-selectivity have been reported. The first highly Z-selective catalysts, based on molybdenum and tungsten, were developed by Schrock and Hoveyda.^{14–16} More recently, ruthenium-based counterparts, containing an N-heterocyclic carbene (NHC) chelated to the metal center via a Ru–C bond, were discovered by Grubbs and co-workers.^{17–19} Highly Z-selective ruthenium-based catalysts were also developed by Hoveyda and co-workers, by replacing the chloride ligands of the Hoveyda–Grubbs second-generation catalyst with a dithiolate ligand.^{20–22}

Computational studies of Grubbs-type catalysts show that the incoming olefin binds the metal center in the *trans*-position with respect to the bulky spectator ligand (e.g., alkyl phosphine or NHC),^{23–33} where also the metallacyclobutane (MCB) intermediate has been experimentally proven to form.^{34–39} In

contrast, the above-mentioned Z-selective ruthenium-based catalysts prefer a side-on or *cis*-bound olefin (see Figure 1).^{20,22,40} An alternative Z-selective catalyst, containing an aryl monothiolate ligand (**1**, Figure 1), was computationally designed and developed in our group, specifically to resemble the parent Grubbs catalysts and to maintain the *trans*-binding of the olefin.³⁸ This compound was obtained through simple substitution of one of the anionic chloride ligands of the Hoveyda–Grubbs second-generation catalyst by 2,4,6-triphenylbenzenethiolate.⁴¹

Upon exchange of the remaining anionic chloride ligand of **1** with isocyanate, catalyst **2** was obtained. This catalyst is surprisingly robust, and it can be used in air without the necessity of solvent and substrate purification.⁴² Furthermore, it tolerates acidic additives under an argon atmosphere while maintaining appreciable Z-selectivity. These conditions (air or acid) significantly reduce the isomerization of the substrate and product that accompanies many transformations.^{42,43} In contrast **1**, which displays a similar tendency to isomerize substrate and products, decomposes rapidly under the same conditions.⁴²

The Z-selectivity of our catalysts **1** and **2** is determined by steric repulsion between the bulky thiolate, effectively shielding one face of the molecule *trans* to the NHC, and the reacting

Received: March 17, 2016

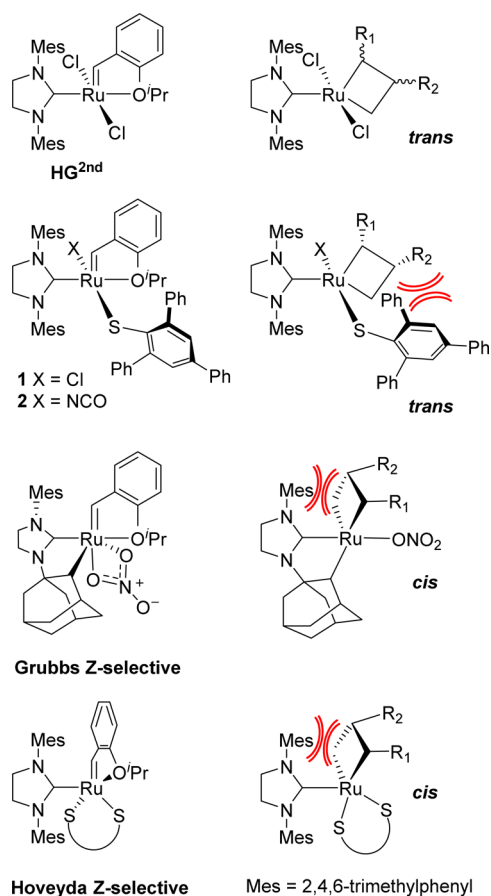


Figure 1. Positioning (*cis* or *trans* with respect to the NHC ligand) of the metallacyclobutane moiety in the catalytic cycle of the Hoveyda–Grubbs second-generation catalyst and of various *Z*-selective ruthenium-based catalysts.

metallacyclobutane moiety and its substituents, R^1 and R^2 (Figure 2). A sterically demanding thiolate thus gives higher

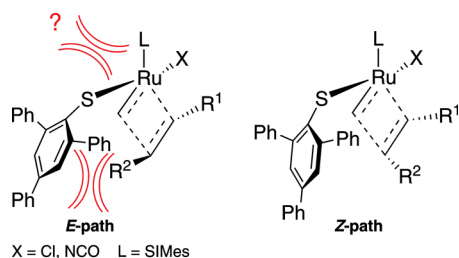


Figure 2. The *E*-path is destabilized with respect to the *Z*-path by the steric repulsion (shown in red) between the arylthiolate and the metallacyclobutane reacting moiety and possibly also by the interactions between the donor *L*-ligand and the thiolate. The importance of the latter interactions (indicated by a question mark) is studied in this work.

Z-selectivity than a small thiolate.³⁸ Also, as indicated in Figure 2, one may also speculate that these thiolate–metallacyclobutane interactions are influenced by the donor *L*-ligand, even if the latter is positioned *trans* to the metallacyclobutane. Clearly, a very small *L*-ligand would allow the thiolate to bend upward, away from the reacting moiety, resulting in complete loss of selectivity. However, the effect of the *L*-ligand on the *Z*-selectivity has so far not been systematically studied and is

poorly understood. It is not known how *L*-ligands with different steric requirements than the SIMes ligand of **1** and **2** would influence the selectivity.

Thus, in order to study the effect of the *trans*-positioned *L*-ligand on the selectivity, and also, more generally, to explore the generality of our catalyst design, we decided to investigate whether “first-generation” versions (i.e., based on phosphine instead of NHC ligands) of the *Z*-selective ruthenium-thiolate catalysts can be obtained and, if so, to what extent they are active and selective. Progress to this end could offer additional molecular “handles” to control and improve the selectivity and other properties of the *Z*-selective monothiolate catalysts.

Some effect of changing the *L*-ligand should be expected simply by considering the well-known fact that the nature of the remaining neutral donor ligand (e.g., NHC or phosphine) strongly influences the catalytic properties of Grubbs-type catalysts.^{44,45} Thus, a key motivation of this work was to investigate the influence of a different class of neutral donor ligands on the selectivity, activity, and stability of the ruthenium arylthiolates.

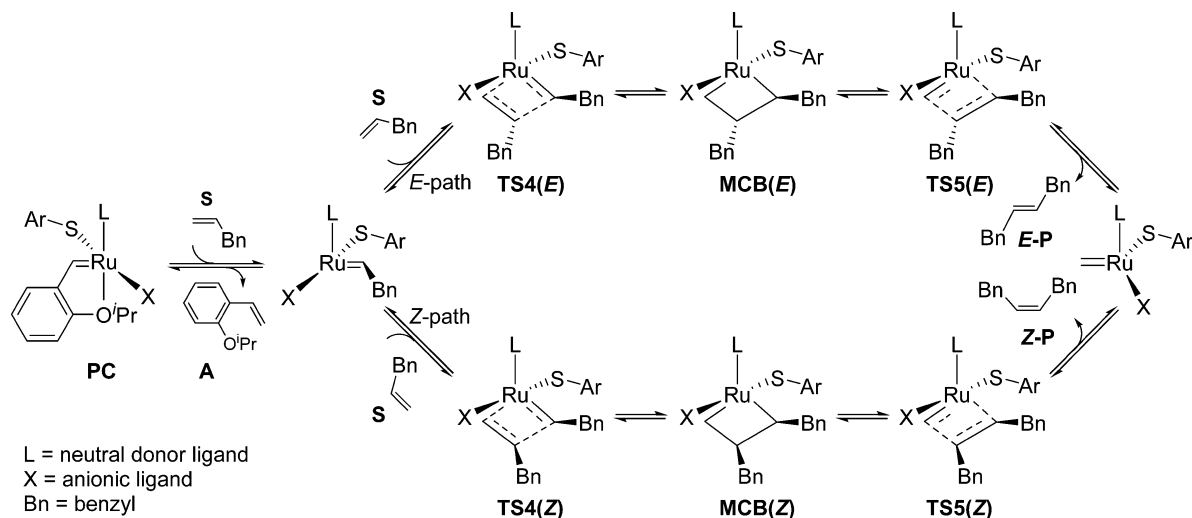
Although second-generation Grubbs catalysts are very active in general, first-generation catalysts are less prone to secondary metathesis reactions and double-bond migration.^{46,47} In addition, phosphine ligands have steric properties different from those of the NHCs, which could modify the thiolate–substituent interactions (Figure 2) and thus the selectivity compared to that of **1** and **2**. A number of phosphine ligands with strongly varying steric properties are commercially available, making this class of ligands particularly tempting for exploration of *Z*-selectivity in combination with arylthiolates. Chen and co-workers have recently shown that the *Z*-selectivity of Ru-based catalysts containing a bidentate *o*-(alkylarylphosphino)phenolate ligand is influenced by the steric nature of the second anionic ligand.^{48,49} In particular, when the chloride was replaced by a sterically demanding thiosulfonate ligand, they observed an increased *cis*-content of the formed C–C double bonds. The same group has also investigated the replacement of chloride by several thiolate ligands, but they found lower *Z*-selectivities than with thiosulfonates.⁵⁰ Even if the best recorded *cis*-content was rather modest (<50%), these results demonstrate that it is possible to make *Z*-selective catalysts based on phosphine ligands and that prefer a bottom attack of the incoming olefin.

In general, the *Z*-selectivity and activity of new phosphine-based catalysts were first assessed computationally, using density functional theory (DFT), and next followed up by synthesis and catalytic tests.

RESULTS AND DISCUSSION

In the following we will try to arrive at improved *Z*-selective phosphine-based catalysts by using computational chemistry and experimental follow up in a sequence of prediction–realization iterations. Each iteration will start by molecular-level calculations to give insight and specific predictions to be followed up by synthesis and testing. The latter will, in turn, serve as feedback to the computational predictions of the next iteration.

The preferred pathways toward the formation of the *E*- and *Z*-olefin are shown in Scheme 1.^{38,39} A computational study of *Z*-selective propene metathesis using **1** shows that the MCB, obtained from cycloaddition via **TS4**, is less stable than the precatalyst (**PC**).³⁹ The rupture of the MCB via **TS5** is energetically more demanding than its formation via **TS4**,³⁹

Scheme 1. Pathways Leading from Initiation to Product^a

^aPC = precatalyst, S = substrate, A = 2-isopropoxystyrene, TS4 = transition state for the cycloaddition, MCB = metallacyclobutane, and TSS(E) and TSS(Z) are the transition states for rupture of the MCB leading to the E (E-P) and Z (Z-P) product, respectively.

which makes TS5 the rate-limiting step. Therefore, the difference in calculated free energy at TS5 between the E- and Z-path, that is, the energy difference between TSS(E) and TSS(Z) ($\Delta\Delta G_{\text{Tol}}^{\ddagger} = \Delta G(E)_{\text{Tol}}^{\ddagger} - \Delta G(Z)_{\text{Tol}}^{\ddagger}$), is used as the computational measure of Z-selectivity.

The TSS(E) and TSS(Z) transition structures of Figure 2 are energetically favored with respect to the two alternative isomers where the R¹ substituent points toward the thiolate.^{38,39,42} Therefore, only the isomers with R¹ directed away from the thiolate were considered in this study, and steric interaction between R¹ and the thiolate is assumed to not contribute to selectivity differences between the catalysts studied in this work. The catalytic activity is approximated by the absolute barrier from the precatalyst (PC) to the most favorable route (TSS(Z)) via TS5. The calculations were performed using allylbenzene as substrate and toluene as solvent.

First-Generation Analogue of 1. In order to obtain initial insight into the role of the donor ligand (L) in controlling the stereoselectivity, we started with a computational evaluation of a variant of 1 bearing a very small L, trimethylphosphine, in combination with a bulky 2,4,6-triphenylbenzenethiolate (3, Figure 3).

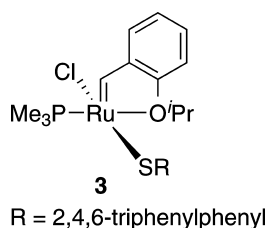


Figure 3. Hoveyda-style catalyst with sterically nondemanding phosphine ligand and bulky 2,4,6-triphenylbenzenethiolate.

A negative energy difference ($\Delta\Delta G_{\text{Tol}}^{\ddagger} = -0.8$ kcal/mol), computed for 3, shows preference for the E-path. That this complex should be E-selective may seem surprising given the presence of the large, presumably selectivity-inducing 2,4,6-triphenylbenzenethiolate ligand also found in 1. However, the small trimethylphosphine ligand allows the thiolate ligand to

twist around the Ru–S and S–Ar bonds. This causes a reduction in steric repulsion between the thiolate ligand and the substituent (R² in Figure 2) on the metallacyclobutane reacting moiety that is pointing toward the thiolate. In other words, the twisting allows for relaxation of the steric repulsion between the thiolate and the forming E-olefin, allowing the transition state of the E-path (TSS(E)), in spite of the fact that R² points toward the thiolate, to be lower in energy than the Z-counterpart. In order to destabilize the E-path, the steric repulsion between the thiolate and the forming olefin must be increased.

To achieve this repulsion, the L-ligand should be bulky enough so as to prevent the thiolate ligand from twisting around the Ru–S and S–Ar bonds. In other words, in the case of phosphine ligands, the P–Ru–S–Ar torsion angle (τ , Figure 4) should be as close to 180° as possible, whereas the Ru–S–C4–C5 torsion (φ , Figure 4) ideally should be 90°. Figure 4 shows that 4, an analogue of 3 equipped with the more bulky tricyclohexylphosphine ligand, reduces the twisting around the R–S bond by 37° ($\tau = -174^\circ$, compared to $\tau = -137^\circ$ in 3) and around the S–Ar bond by 25° ($\varphi = -90^\circ$, compared to $\varphi = -115^\circ$ in 3). This ensures Z-selectivity, but the predicted Z-selectivity for complex 4 ($\Delta\Delta G_{\text{Tol}}^{\ddagger} = 0.9$ kcal/mol) is still significantly lower than that of 1 ($\Delta\Delta G_{\text{Tol}}^{\ddagger} = 3.1$ kcal/mol). In addition, the tricyclohexylphosphine complex also has a much higher calculated absolute barrier (i.e., TSS(Z) calculated from PC) to olefin metathesis ($\Delta G(Z)_{\text{Tol}}^{\ddagger} = 28.0$ kcal/mol in 4 vs 18.8 kcal/mol in 1), suggesting that 4 should be a less active catalyst than 1.

Even though the calculated indicators of the first-generation analogue 4 were not very promising, we decided to proceed with the experimental work. The synthesis of 4 was expected to be straightforward, and this compound could thus offer a quick initial feedback on the accuracy of the calculations for the phosphine-based Z-selective catalysts. Indeed, the first-generation analogue 4 (Scheme 2) of 1 was easily prepared by reacting the commercially available Hoveyda–Grubbs first-generation catalyst with potassium 2,4,6-triphenylbenzenethiolate in tetrahydrofuran (THF) at room temperature.

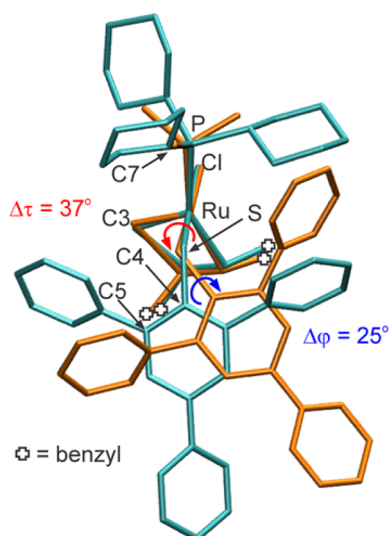
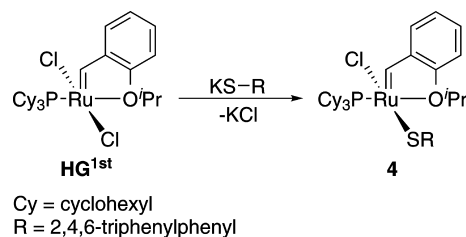


Figure 4. Comparison between the P–Ru–S–Ar (τ) and the Ru–S–C4–C5 (ϕ) torsion angles in **3** and **4**. The two structures have been fitted using the Quatfit program⁵¹ with the following weights: 10^8 for Ru, 10^7 for P, C3, and Cl. Only these four pairs of atoms were included in the fitting procedure.

Scheme 2. Synthesis of Compound **4**



Dark red crystals of **4** suitable for X-ray structure analysis were grown at low temperature ($-32\text{ }^\circ\text{C}$) from a THF/*n*-pentane solution. Its molecular structure and relevant bond lengths and angles are shown in Figure 5. The compound can be described as a slightly distorted square pyramid with the alkylidene ligand occupying the apical position. Of the remaining ligands occupying basal positions the thiolate moiety is *trans* to the chloride ligand (Cl1) and the phosphine (P1) is *trans* to the oxygen atom of the isopropoxy ligand (O1). Bond lengths and angles of the moieties found in both **1** and **4** are comparable, the most noticeable difference being the Ru1–S1–C1 angle, which is somewhat wider in **4** (117° vs 113° ⁴¹).

Catalytic tests of **4** and **1** in metathesis homocoupling reactions (Table 1) reveal lower activity and *Z*-selectivity compared to **1**. This is in qualitative agreement with the above calculated barriers.

As discussed above, the DFT calculations revealed that the tricyclohexylphosphine, in contrast to the smaller trimethylphosphine, ligand is able to orient the thiolate downward, enough to ensure moderate *Z*-selectivity. Here, we will analyze the geometries in more detail, to shed some light on the origin of the lower *Z*-selectivity of **4** with respect to **1**. First of all, as already seen in the validation against X-ray structures of ruthenium pre-catalysts,⁵² geometries optimized using the ω B97XD functional (applied here) compare well with the corresponding structures obtained from single-crystal X-ray diffraction. This is also true for the angles defining the position of the arylthiolate. For example, the calculated (experimental)

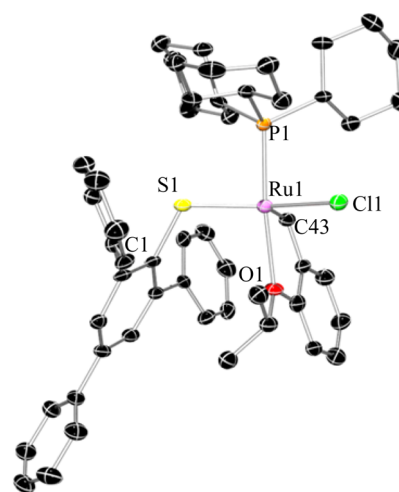


Figure 5. X-ray structure of **4** with displacement ellipsoids drawn at the 50% probability level. H atoms and solvent molecule (*n*-pentane) are omitted for clarity. Selected geometrical parameters: Ru1–C43 = 1.840(8) Å, Ru1–P1 = 2.284(2) Å, Ru1–Cl1 = 2.358(2) Å, Ru1–O1 = 2.303(5) Å, Ru1–S1 = 2.276(2) Å, Ru1–S1–C1 = $117.0(3)^\circ$, P1–Ru1–S1 = $88.27(7)^\circ$, P1–Ru1–Cl1 = $90.21(7)^\circ$, S1–Ru1–Cl1 = $150.21(8)^\circ$, P1–Ru1–O1 = $174.4(1)^\circ$.

Table 1. Comparison of **1** and **4** in Metathesis Homocoupling

entry	cat	sub ^a	<i>t</i> (h)	conv ^b (%)	yield ^b (%)	<i>Z</i> ^b (%)
1 ^c	1	ATMS	18	22	12	95
2 ^c	4	ATMS	68	3	2.5	87
3 ^d	1	AB	1	7	5	85
4 ^e	4	AB	1	1	0.2	n.d.
			16	9	1	61

^aATMS = allyltrimethylsilane, AB = allylbenzene. ^bDetermined by ¹H NMR analysis. Conversion is the amount of substrate converted, whereas yield refers to the amount of substrate converted into metathesis homocoupling products. For entries 3 and 4 the difference between conversion and yield corresponds to the amount of 1-alkene to 2-alkene isomerization of the substrate. For entries 1 and 2 the difference is due to the 1-alkene to 2-alkene isomerization of the substrate (major product) and to the cross metathesis products between the substrate and its 2-alkene isomer (minor product). ^cCatalyst loading = 0.25 mol %, 4 M in THF, *T* = 60 °C. ^dCatalyst loading = 0.1 mol %, neat substrate, *T* = 20 °C. ^eCatalyst loading = 1 mol %, neat substrate, *T* = 20 °C.

P–Ru–S angle in the pre-catalyst of **4** is 88° (88°), while the Ru–S–C(Ar) angle is 115° (117°). In comparison, the NHC ligand of **1** is better at pushing the thiolate down toward the site to which the olefin binds, with the C(NHC)–Ru–S angle being 92° (91°) and the Ru–S–C(Ar) angle being 112° (113°). A more downward bent thiolate in **1** is also seen in the optimized selectivity-determining transition states (TSS), with a C(NHC)–Ru–S angle for the *E*-path (*Z*-path) equal to 89° (90°) and the Ru–S–C(Ar) angle being 115° (109°), compared to 85° (86°) and 116° (109°), respectively, for **4**.

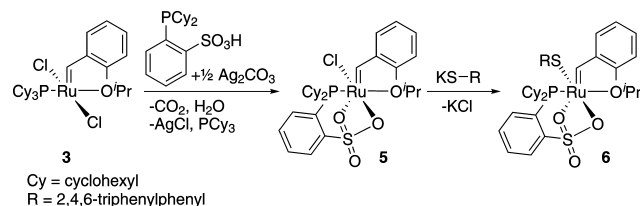
One might speculate that part of the lower selectivity of **4** compared to **1** could be due to relaxation of the *E*-olefin/thiolate steric repulsion via rotation of the tricyclohexyl ligand around the P–Ru bond. Indeed, the analysis of geometries of the optimized transition states TSS(*E*) and TSS(*Z*) for **4** shows that the phosphine ligand is rotated by 13° (as measured using the C3–Ru–P–C7 angle, Figure 4) around the Ru–P bond in

TSS(*E*) with respect to its orientation in TSS(*Z*). In comparison, the NHC ligand in **1** rotates much less (1°) between *E*- and *Z*-transition states.

Restricting Phosphine Rotation Using a P–O Chelate.

Claverie and co-workers recently reported olefin metathesis catalysts bearing chelating phosphine sulfonates.⁵³ Encouraged by these results, we performed DFT calculations showing promising *Z*-selectivity for a complex (**6**, Scheme 3) containing

Scheme 3. Two-Step Synthesis of Compound **6**



such a ligand. The measure of *Z*-selectivity, $\Delta\Delta G^\ddagger_{\text{Tot}} = 2.6$ kcal/mol, for this complex is not much lower than that of **1**. A phosphine rotation of only 1° is seen between the TSS *E*- and *Z*-transition states, confirming robustness against relaxation of phosphine–thiolate steric interactions. However, the slightly higher $\Delta G(Z)^\ddagger_{\text{Tot}}$ of **6** (22.0 kcal/mol) compared to **1** indicates that a somewhat lower catalytic activity can be expected.

Reaction of *o*-(dicyclohexylphosphino)sulfonic acid with half an equivalent of Ag_2CO_3 in THF produces the required silver salt *in situ* (Scheme 3).⁵⁴ Subsequent addition of the Hoveyda–Grubbs first-generation catalyst gives a mixture of the precursor compound **5** and the starting complex. The final product **6** was obtained after reaction of purified **5** with potassium 2,4,6-triphenylbenzenethiolate. Diffusion of *n*-pentane into a concentrated solution of **6** in dichloromethane at low temperature (-32°C) yielded dark green crystals suitable for X-ray structure analysis. The molecular structure and relevant bond lengths and angles are shown in Figure 6.

With the sulfonate moiety bound to ruthenium in a $\kappa^2\text{O},\text{O}'$ fashion, **6** is formally an 18-electron complex with a distorted octahedral structure. The two sulfonate oxygen atoms (O1, O2) are coordinated *trans* to the thiolate (S2) and *trans* to the alkylidene, respectively. In agreement with the expected stronger *trans*-influence of the alkylidene, the O1–Ru (2.171 Å) is significantly shorter than the O2–Ru (2.424 Å) bond. This, in turn gives a somewhat longer S1–O1 (1.493 Å) than S1–O2 (1.464 Å) bond. The other bond lengths are comparable to those of **4**, with the exception that the Ru1–O4 bond of the isopropoxy group is longer (2.345 vs 2.304 Å in **4**), presumably as a result of hexacoordination. The bond angle formed by the thiolate sulfur ($\text{Ru1–S2–C19} = 112^\circ$) is slightly sharper than that in **1** (113°).⁴¹

Surprisingly, and in spite of a relatively low calculated absolute barrier to olefin metathesis ($\Delta G(Z)^\ddagger_{\text{Tot}} = 22.0$ kcal/mol), compound **6** turned out to be completely inactive in homocoupling of allylbenzene at room temperature (entry 3, Table 2) and at 40°C (entry 4). Whereas only some isomerization of the substrate was observed at 60°C , further temperature increases led to olefin metathesis products, mainly of the *E*-isomer, presumably as a result of decomposition of **6** into catalytically active species (entry 6). Similarly, it is also possible to activate **6** using acid to give a catalyst that is not *Z*-selective. An experiment similar to entry 3 except for the use of

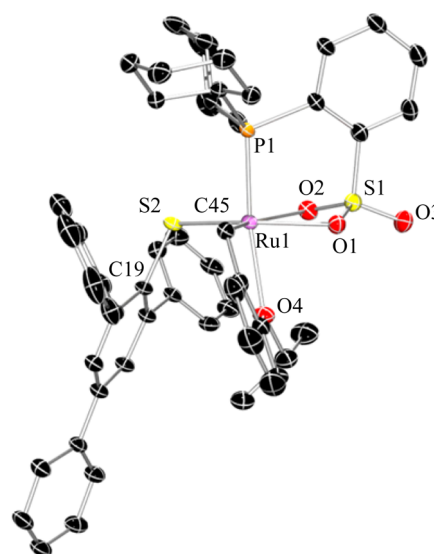


Figure 6. X-ray structure of **6** with displacement ellipsoids drawn at the 50% probability level. H atoms and solvent molecule (dichloromethane) are omitted for clarity. Selected geometrical parameters: Ru1–C45 = 1.8501(2) Å, Ru1–P1 = 2.2790(5) Å, Ru1–O1 = 2.1706(1) Å, Ru1–O2 = 2.4236(2) Å, Ru1–O4 = 2.3448(2) Å, Ru1–S2 = 2.2886(5) Å, S1–O1 = 1.4931(2) Å, S1–O2 = 1.4641(2) Å, S1–O3 = 1.4321(2) Å, Ru1–S2–C19 = $112.41(6)^\circ$, P1–Ru1–S2 = $89.138(2)^\circ$, P1–Ru1–O1 = $93.29(4)^\circ$, P1–Ru1–O2 = $83.25(4)^\circ$, P1–Ru1–O4 = $169.66(4)^\circ$, S2–Ru1–O1 = $157.44(4)^\circ$.

Table 2. Homocoupling of Neat Allylbenzene

entry	cat ^a	T (°C)	t (h)	conv ^b (%)	yield ^b (%)	Z ^b (%)
1	1 ^c	20	1	7	5	85
2	4	20	1	1	0.2	n.d.
			16	10	1	61
3	6	20	1	0	0	
4	6	40	1	0	0	
5	6	60	1	1	0	
6	6	80	1	73	9	29
			24	100	7	29
7	8a	20	1	60	2	50
8	8b	20	1	21	13	81

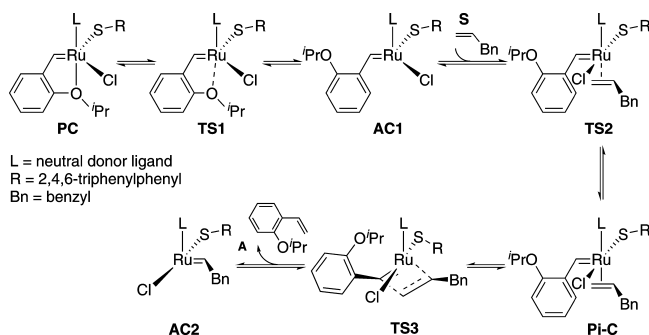
^aCatalyst loading = 1 mol %. ^bDetermined by ^1H NMR analysis. Conversion is the amount of substrate converted, whereas yield refers to the amount of substrate converted into metathesis homocoupling products. The difference between conversion and yield corresponds to the amount of 1-alkene to 2-alkene isomerization of the substrate. ^cCatalyst loading = 0.1 mol %.

2 equiv of phenylphosphoric acid gave 22% conversion, 21% yield, and 21% *Z*.

In addition to the fact that the $\kappa^2\text{O},\text{O}'$ -binding of the sulfonate provides electronic saturation (with an electron count of 18) and adds steric congestion around ruthenium, the bulky thiolate ligand, forming an even sharper angle ($\text{Ru1–S2–C19} = 112^\circ$) with ruthenium than in **1**, projects significant steric pressure toward the site located *trans* with respect to the phosphorus atom, seemingly shielding the catalytic site. Thus, at least at first glance, the electronic saturation and steric congestion together are consistent with low or no activity for **6**, whereas less sterically congested compounds (similar to precursor **5**) containing chelating phosphine sulfonate ligands are in fact active in olefin metathesis.⁵³

In order to possibly shed some light on the reasons for the inactivity of **6**, additional DFT calculations were performed on both **1** and **6**. One potential cause for the lack of activity could be a prohibitively high barrier to initiation. Whereas a computational study of propene metathesis using **1** showed **TS5** to be the selectivity-determining barrier of the regular catalytic cycle, the transition state for formation of the **MCB** intermediate during the initiation stage (**TS3**, Scheme 4) was

Scheme 4. Pathway from Precursor to Active Catalyst^a



^aPC = precatalyst, TS1 = transition state for Ru–OⁱPr bond rupture, AC1 = first active complex, S = substrate, TS2 = transition state for olefin coordination, Pi–C = π -complex, TS3 = transition state for **MCB** formation, A = 2-isopropoxystyrene, AC2 = second active complex. The **MCB** and the transition state for rupture of the **MCB**, located between TS3 and AC2, have been omitted for clarity.

found to be the overall highest barrier.³⁹ However, formation of the **MCB** during initiation seems to be easy for **6**, with a lower barrier for **TS3** (calculated with substituents on the same side of the metallacyclobutane, as previously shown to be the most stable isomer of **TS3**)³⁹ than that calculated for **1** (entries 1, 2, Table 3), implying that **TS3** of the initiation cannot explain the

Table 3. Key Stationary Points along the Initiation Path^a

entry	cat.	TS1	AC1	TS2	Pi-C	TS3
1	1	12.0	8.0	22.9	23.9	28.7
2	6	10.0	8.4	21.5	20.0	22.8

^aGibbs free energy [kcal/mol] in toluene.

lack of activity. We thus continued by checking whether the other elementary steps of the initiation (Scheme 4) could be associated with prohibitively high barriers. The first of these involves the rupture of the Ru–OⁱPr bond (**TS1**) according to a dissociative mechanism, but also this barrier is lower for **6** than for **1** (entries 1, 2, Table 3). An alternative interchange mechanism, in which the isopropoxy dissociation is promoted by the incoming olefin, is reported to be competitive for the Hoveyda–Grubbs dichloride catalysts.⁵⁵ However, the bulky arylthiolate ligand of **6** effectively blocks coordination of the olefin prior to isopropoxy dissociation.³⁹

One might think that the next step, the coordination of the olefin, could be hindered by the combination of the bulky groups, the arylthiolate and the sulfonate, enveloping the metal center. However, also this reaction appears to be more facile, with less energy required to reach **TS2** for **6** than for **1**.

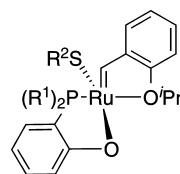
Since both the initiation phase and the catalytic cycle of **6** appear to be relatively facile, the explanation for the lack of activity must be sought elsewhere. The activity combined with lack of selectivity observed at higher temperatures (Table 2)

suggests that, under catalytic conditions, **6** may undergo structural changes, or decomposition, to give catalytically active but unselective species. Of course, it is hard to guess which species or decomposition reactions that are involved. However, we have previously observed that the thiolate ligand weakens the *trans*-positioned Ru–Cl bond in **1**,⁴² and one candidate structural modification thus could be dissociation of the sulfonate ligand of **6**. In other words, if dissociation of the sulfonate is more facile than dissociation of the OⁱPr moiety to form the active complex (**AC**), then the resulting zwitterionic species could be responsible for the catalytic activity observed at higher temperatures. However, the calculated free energy of the zwitterionic species is 22.0 kcal/mol above that of the precatalyst and thus also 12.0 kcal/mol above **TS1**. With also this alternative determined to be unlikely, we can only conclude that the computational mechanistic exploration offered no explanation for the lack of activity and selectivity of **6**.

Reducing the Size of the P–O Chelate. Since the *o*-(dicyclohexylphosphino)sulfonate ligand did not lead to appreciable activity and selectivity, we turned to an alternative class of bidentate phosphine ligands, based on an *o*-(dialkylphosphino)phenolate chelating moiety.⁵⁶ Chen and co-workers have recently used this kind of ligand to develop a new family of highly active ruthenium–alkylidene olefin metathesis catalysts for copolymerization of norbornene and cyclooctene.^{48,49} They have also shown that a sterically demanding second anionic ligand (in combination with the chelating phosphino phenolate) leads to increased *cis*-content of C–C double bonds in the resulting copolymer.

Encouraged by the *Z*-selectivity and activity observed by Chen and co-workers, and still with the goal to hinder rotation of the phosphine and improve upon the design of complex **6**, we decided to explore the *o*-(dialkylphosphino)phenolate ligand. Also encouraging is the fact that the five-membered ring formed by an *o*-(dialkylphosphino)phenolate with ruthenium (Ru–P–aryl–O) represents a less sterically demanding second anionic ligand, to be used in combination with a large arylthiolate, than the six-membered Ru–P–aryl–SO₃ ring in **6**. Even if the reasons for the lack of activity and selectivity of the latter catalyst could not be determined, it is intuitively promising that the phenolate moiety can be expected to bind ruthenium in $\kappa^1\text{O}$ fashion only and thus avoid formation of an 18-electron complex as in **6**.

In combination with the relatively compact Ru–P–aryl–O chelating moiety, we opted to equip the phosphorus atom with sterically demanding *tert*-butyl substituents to help push the arylthiolate down toward the olefin-binding site (**8b**, Figure 7), cf. the mechanism of Figure 2. To help evaluate this expected selectivity-boosting phosphine–thiolate repulsion, we also



- 8a** R¹ = *tert*-butyl, R² = 2,4,6-trimethylphenyl
8b R¹ = *tert*-butyl, R² = 2,4,6-triphenylphenyl
9 R¹ = cyclohexyl, R² = 2,4,6-triphenylphenyl
10 R¹ = 1-adamantyl, R² = 2,4,6-triphenylphenyl

Figure 7. Compounds **8**–**10**, bearing *o*-(dialkylphosphino)phenolate ligands.

included the smaller 2,4,6-trimethylbenzenethiolate ligand (**8a**) and two variants of **8b**, one with somewhat less sterically demanding alkyl groups (cyclohexyl) on phosphorus (**9**) and one with somewhat more sterically demanding alkyl groups (1-adamantyl) on phosphorus (**10**).

The calculated activities and selectivities of compounds **8a**, **8b**, **9**, and **10** are given in Table 4. The catalyst with *o*-(di-*tert*-

Table 4. Comparison of Computed Parameters of the OM Catalysts with **1**

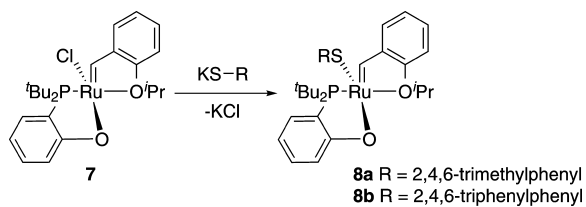
entry	cat	$\Delta\Delta G_{\text{Tol}}^{\ddagger a}$	$\Delta G(Z)_{\text{Tol}}^{\ddagger b}$
1	1	3.1	18.8
2	3	-0.8	n.a.
3	4	0.9	28.0
4	6	2.6	22.0
5	8a	0.3	26.3
6	8b	1.6	24.8
7	9	0.8	26.7
8	10	1.5	n.a.

^aThe relative energies [kcal/mol] are a measure of *Z*-selectivity; $\Delta\Delta G_{\text{Tol}}^{\ddagger} = \Delta G(E)_{\text{Tol}}^{\ddagger} - \Delta G(Z)_{\text{Tol}}^{\ddagger}$. ^b $\Delta G(Z)_{\text{Tol}}^{\ddagger}$ is the absolute barrier to TSS(*Z*) with the precatalyst **PC** as the reference.

butylphosphino)phenolate (**8b**, entry 6) appears to be a promising candidate. Although the measure of selectivity ($\Delta\Delta G_{\text{Tol}}^{\ddagger}$) is only about half that of **1**, it is higher than that obtained for **4**, **8a**, **9**, and **10** (entries 5, 7 and 8, Table 4). Furthermore, the absolute barrier ($\Delta G(Z)_{\text{Tol}}^{\ddagger}$) calculated for **8b** is lower than for the other catalysts (except **1**), suggesting that this compound could be a reasonably active catalyst. Surprisingly, in spite of the adamantyl groups of **10** presumably being even more sterically demanding than the *tert*-butyl groups of **8b**, the calculated selectivity of **10** is essentially the same as that of **8b**. This, the unexpectedly low $\Delta\Delta G_{\text{Tol}}^{\ddagger}$ of **10**, results from the solvent corrections (see the Supporting Information for tabulated relative energies and enthalpies and the various thermochemical and solvent corrections), which favor the *E*-path. In other words, the intramolecularly induced selectivity of **10**, reflected in the gas-phase-calculated $\Delta\Delta G^{\ddagger}$ (= 2.1 kcal/mol), is, as expected, higher than that of **8b** (1.2 kcal/mol).

As seen above, in solution **8b** and **10** are predicted to be equally selective, which means that other factors must count when selecting which compound to synthesize. Due to the lower cost of preparing the *o*-(di-*tert*-butylphosphino)phenolate ligand, we decided to synthesize **8b**. For comparison, the closely related **8a** was also selected for experimental follow up since the thiol is commercially available and the synthesis was not expected to require much extra work. Precursor **7** (Scheme 5) and the *o*-(di-*tert*-butylphosphino)phenolate ligand necessary to synthesize **7** were prepared according to literature procedures.^{49,57} The final products were obtained after reaction

Scheme 5. Synthesis of Compounds **8a** and **8b**



of **7** with potassium 2,4,6-trimethylbenzenethiolate (**8a**) and potassium 2,4,6-triphenylbenzenethiolate (**8b**), respectively.

Diffusion of *n*-pentane into a concentrated solution of **8b** in dichloromethane at low temperature ($-32\text{ }^{\circ}\text{C}$) yielded dark red crystals suitable for X-ray structure analysis. Its molecular structure and relevant bond lengths and angles are shown in Figure 8. Compound **8b** can be described as a slightly distorted

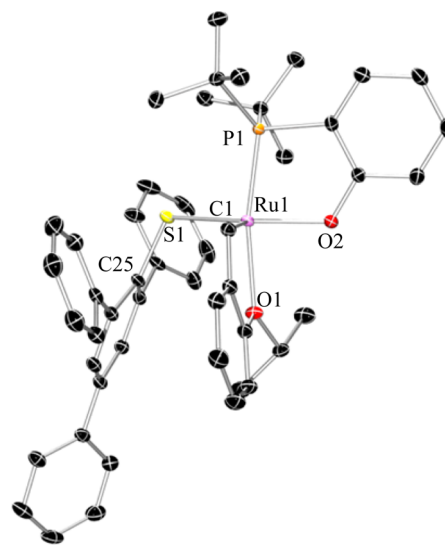


Figure 8. X-ray structure of **8b** with displacement ellipsoids drawn at the 50% probability level. H atoms and solvent molecule (dichloromethane) are omitted for clarity. Selected geometrical parameters: Ru1–C1 = 1.846(2) Å, Ru1–P1 = 2.2653(5) Å, Ru1–O1 = 2.2531(2) Å, Ru1–O2 = 2.0246(2) Å, Ru1–S1 = 2.2846(6) Å, Ru1–S1–C25 = 114.21(7) $^{\circ}$, P1–Ru1–S1 = 92.412(2) $^{\circ}$, P1–Ru1–O1 = 168.79(5) $^{\circ}$, P1–Ru1–O2 = 83.51(4) $^{\circ}$, S1–Ru1–O2 = 152.11(5) $^{\circ}$.

square pyramid with the alkylidene occupying the apical position. Of the remaining ligands occupying basal positions the thiolate moiety is *trans* to the phenoxylate oxygen (O2) and the phosphine (P1) is *trans* to the alkoxy oxygen atom (O1). Bond lengths are comparable to those of **4**, **6**, and **1**.⁴¹ However, the bond distance between ruthenium and the phenolate oxygen (Ru1–O2 = 2.025 Å) is clearly shorter than the corresponding Ru–O_{sulfonate} bond distances (2.304 and 2.345 Å) of complex **6**. Furthermore, the angle between phosphorus and the phenolate oxygen atom (O2) of the sulfonate moiety (P1–Ru1–O2 = 83.51 $^{\circ}$) is smaller than 90 $^{\circ}$. The bond angle around the sulfur atom of the thiolate ligand (Ru1–S1–C25 = 114 $^{\circ}$) is larger than that of **6** (112 $^{\circ}$) but sharper than that of **4** (117 $^{\circ}$).

Catalyst **8a** rapidly converts allylbenzene at room temperature (entry 7, Table 2). However, even though 60% of the allylbenzene was converted after 1 h, only 2% metathesis product was obtained and with only modest *Z*-selectivity (50%). Even though the conversion of **8b** (entry 8) is somewhat lower compared to **8a**, its olefin metathesis yield is much higher than that of both **4** and **8a**, in agreement with the fact that the computational barrier to olefin metathesis, $\Delta G(Z)_{\text{Tol}}^{\ddagger}$ is lower for **8b** than for **8a** and **4**. Perhaps more important, we found that **8b** gave a *Z*-selectivity above 80% in homocoupling of allylbenzene, to our knowledge the highest *Z*-selectivity so far obtained with phosphine-based, first-generation-style catalysts.

Table 5. Homocoupling of Allylbenzene with **8b** under Different Reaction Conditions

entry	cat load (mol %)	additive ^a	solvent	[sub] (M)	T (°C)	t (h)	conv ^b (%)	yield ^b (%)	Z ^b (%)
1	1			neat	20	0.5	10	6	83
						1	21	13	81
						4	69	26	73
2	1			neat	40	4	99	17	26
3	1			neat	60	0.5	97	19	45
4	2			neat	20	1	32	18	82
5	4			neat	20	1	35	19	82
6	1		toluene	4	20	1	9	5	81
7	1		THF	4	20	1	9	3	81
8	1		<i>p</i> -cymene	4	20	1	6	3	82
9	1		toluene	1	20	1	6	1	81
10	1		toluene	2	20	1	6	2	80
11	1		toluene	3	20	1	9	4	81
12	1		toluene	4	40	1	19	11	77
13	1	QUI		neat	20	4	29	28	49
14	1	PPA		neat	20	4	9	4	63
15	1	TCPO		neat	20	4	37	25	81
16	1	H ₂ O		neat	20	4	25	12	81

^aQUI = 2,6-dichloro-1,4-benzoquinone (1 equiv with respect to the cat), PPA = phenyl phosphoric acid (1 equiv with respect to the cat), TCPO = tricyclohexylphosphine oxide (5 equiv with respect to the cat), 1 drop H₂O. ^bDetermined by ¹H NMR analysis. Conversion is the amount of substrate converted, whereas yield refers to the amount of substrate converted into metathesis homocoupling products. The difference between conversion and yield corresponds to the amount of 1-alkene to 2-alkene isomerization of the substrate.

The low *Z*-selectivity obtained with the small thiolate ligand (**8a**) is as predicted (entry 5, Table 4) and shows that the *o*-(di-*tert*-butylphosphine)phenolate, even with its bulky *tert*-butyl groups facing the thiolate, does not induce much selectivity by itself. As expected, the small trimethylbenzene in **8a** allows for relaxation of the steric interaction between the thiolate and the R² substituent (Figure 2) via thiolate twisting around the Ru–S (τ) and S–Ar (φ) bonds as defined in Figure 4. Indeed, TSS(*E*) of **8a** shows the largest departure from the ideal, nontwisted case ($\tau = 180^\circ$ and $\varphi = -90^\circ$) for both Ru–S ($\tau = -165^\circ$ vs $\tau = -168^\circ$ in **8b**, $\tau = -178^\circ$ in **9**, and $\tau = 178^\circ$ in **10**) and S–Ar ($\varphi = -99^\circ$ vs $\varphi = -94^\circ$ in **8b**, $\varphi = -88^\circ$ in **9**, and $\varphi = -85^\circ$ in **10**) among the complexes with *o*-(dialkylphosphino)phenolate chelating moieties. This twisting allows **8a** to have a wide P–Ru–S angle (95° vs 94° in **8b**, 90° in **9**, and 95° in **10**) and a sharp Ru–S–C(Ar) angle (113° vs 114° in **8b**, 113° in **9**, and 113° in **10**) without this being reflected in high selectivity.

From the above we can conclude that the small thiolate allows for relaxation of the metallacyclobutane–thiolate repulsion, which decreases *Z*-selectivity. Therefore, increasing the size of the thiolate, by introducing phenyl substituents on the benzene ring as in **8b**, seems to be the key selectivity-inducing element.

Catalysis Using **8b under Different Reaction Conditions.** A series of experiments with varying catalyst loading, solvent, substrate concentration, reaction temperature, and additives were performed using **8b**. Whereas a complete overview of these results is given in Table S1 of the Supporting Information, a summary is included in Table 5. The best conditions seem to be a temperature of 20 °C, with 1 mol % catalyst in neat substrate using 5 equiv of tricyclohexylphosphine oxide (TCPO) as additive. Further conclusions from these experiments are described in the following:

- Isomerization of the substrate is promoted by increasing temperature, especially at high substrate conversion (entries 1–3).

- Increasing the catalyst loading leads to only slight improvement in *Z*-isomer yield (i.e., the product of the yield and percentage of *Z*-isomeric product, entries 1, 4, 5).

- Using solvents (entries 6–8) invariably results in lower conversion and yield than catalysis in neat allylbenzene (entry 1). Only insignificant differences between the various solvents are observed.

- Reduced substrate concentration leads to lower conversion and yield (entries 9–12).

Several additives were tested: 2,6-dichloro-1,4-benzoquinone effectively prevents isomerization (entry 13), but unfortunately at the expense of a sharp decline in *Z*-selectivity. Phenylphosphoric acid gives low conversion and yield and only moderate *Z*-selectivity (entry 14). Tricyclohexylphosphine oxide and water (entries 15, 16) prevent isomerization of the *Z*-product in the *E*-product, resulting in persistent, high *Z*-selectivity at longer reaction times. Unfortunately, when using water as additive, the progress of the reaction stops at ca. 25% substrate conversion, indicating inactivation or decomposition of the catalyst.

Catalysis Using Different Substrates. Catalysts **8a** and **8b** were tested in several neat substrates other than allylbenzene to determine tolerance toward different functional groups (Table 6). For substrates particularly prone to isomerization, TCPO was added to attempt to maintain *Z*-selectivity and yield as described above for allylbenzene (Table S1). For **8a**, yield and *Z*-selectivity remained low, as expected, and addition of TCPO did not improve the *Z*-selectivity but to some extent suppressed isomerization of the substrate (entries 3, 4). For allyltrimethylsilane (entry 6), addition of TCPO led to complete lack of catalytic activity.

Interestingly, high *Z*-selectivity, moderate yield, and only negligible isomerization of the substrate were obtained with **8b** in 1-octene and allyl acetate (entries 7 and 8). In contrast, the corresponding *Z*-selectivity in 2-allyloxyethanol (entry 9) is low and comparable to that obtained with **8a**, presumably due to

Table 6. Homocoupling of Various Neat Substrates

entry	cat ^a	sub ^b	additive ^c	t (h)	conv ^d (%)	yield ^d (%)	Z ^d (%)
1	8a	AB	TCPO	8	95	6	38
2	8a	AAc		1	5	5	34
3	8a	AOE		1	12	2	65
4	8a	AOE	TCPO	1	1.4	0.8	66
				48	98	4	44
5	8a	ATMS		1	1	0.5	88
6	8a	ATMS	TCPO	1	0		
				48	0		
7	8b	OCT		1	4	4	82
				4	10	10	82
				8	27	27	82
8	8b	AAc		1	6	6	95
				4	16	16	93
				8	24	24	92
9	8b	AOE		1	3	2	54
				4	6	3	54
				8	8	3	54
10	8b	AOE	TCPO	8	8	4	74
				48	19	8	74
11	8b	PB		1	14	12	80
				4	45	30	77
				8	77	36	71
12	8b	PB	TCPO	8	43	34	79
				24	71	47	74

^aCatalyst loading = 1 mol %, $T = 20\text{ }^{\circ}\text{C}$. ^bAB = allylbenzene, OCT = 1-octene, AAc = allyl acetate, AOE = 2-allyloxyethanol, ATMS = allyltrimethylsilane, PB = 4-phenyl-1-butene. ^cTCPO = tricyclohexylphosphine oxide (5 equiv). ^dDetermined by ¹H NMR analysis. Conversion is the amount of substrate converted, whereas yield refers to the amount of substrate converted into metathesis homocoupling products. For entries 1, 3, 4, 9, and 10 the difference between conversion and yield corresponds to the amount of 1-alkene to 2-alkene isomerization of the substrate. For entry 5 the difference is due to the 1-alkene to 2-alkene isomerization of the substrate (major product) and to the cross metathesis products between the substrate and its 2-alkene isomer (minor product).⁴⁰ For entries 11 and 12 the difference is mainly due to the 1-alkene to 2-alkene isomerization of the substrate. In addition, small amounts of cross metathesis products between the substrate and its 2-alkene isomer as well as of compounds resulting from double-bond migration in the target homocoupling product were detected.

isomerization. Addition of TCPO improved the Z-selectivity (entry 10). The yield and Z-selectivity obtained with 8b in 4-phenyl-1-butene (entries 11, 12) are comparable to those observed above with allylbenzene.

Importantly, and in contrast to results for NHC-based catalysts, only negligible or little Z–E isomerization of the product is observed with 8b with increasing substrate conversion. The sustained Z-selectivity is probably due to low activity in secondary metathesis, since this trend is observed also when the Z-selectivity is moderate (e.g., entries 8 and 9).

Ring-Opening Metathesis Polymerization (ROMP). In addition to the above-described homocoupling reactions, our catalysts were tested in ROMP of neat *cis*-cyclooctene (Table 7). The conditions optimal for homocoupling of terminal olefins were applied also in ROMP. In general, the resulting activities were low and the Z-selectivities only moderate, even though the latter were still clearly higher than that of the Hoveyda–Grubbs first-generation catalyst (entry 1) and comparable to, or slightly higher than, those of related

Table 7. ROMP of *cis*-Cyclooctene at 20 °C

entry	cat	cat load (mol %)	t (h)	yield ^a (%)	Z ^a (%)
1	HG ^{first}	1	16	100	24
2	4	1	16	6	47
3	6	1	16	1	47
4	8a	1	16	0.5	67
5	8b	1	16	13	54

^aDetermined by ¹H NMR analysis.

complexes based on a chelating *o*-(alkylarylphosphino)-phenolate and a sterically demanding thiosulfonate ligand reported by Chen and co-workers.⁵⁰ The lower selectivity of the latter catalysts may in part be caused by the fact that one of the phosphine substituents, a phenyl, is less sterically demanding than the *tert*-butyl groups of 8a and 8b.

The highest yield was obtained for 8b, in combination with rather low Z-selectivity. 6 and 8a were hardly active in ROMP, but the 1% yield obtained with 6 is still an interesting observation given the fact that this compound was completely inactive in homocoupling at low temperatures.

CONCLUSIONS

We have synthesized and tested phosphine-based ruthenium olefin metathesis catalysts with appreciable Z-selectivity, giving 70–95% of the Z-isomer product in homocoupling of terminal alkenes such as allylbenzene, 1-octene, allyl acetate, and 2-allyloxyethanol, in combination with low to moderate (up to ca. 50%) yields. The Z-selectivity of these catalysts is induced by the presence of a sterically demanding monodentate arylthiolate. They may thus be termed first-generation analogues of our previously reported NHC-based Z-selective ruthenium catalysts bearing monodentate arylthiolate ligands,^{38,41,42} often achieving somewhat lower activities and Z-selectivities than their second-generation counterparts, but also offering examples giving less substrate and product isomerization and thus higher yields.

Both the first- and second-generation versions of the Z-selective ruthenium-based catalysts may be obtained via one or two ligand exchange reactions starting from the corresponding first- or second-generation Hoveyda–Grubbs ruthenium dichloride olefin metathesis catalyst, and they also resemble the “parent” unselective ruthenium catalysts by binding the substrate olefin to form the metallacyclobutane *trans* to the phosphine or NHC donor ligand, L.

Geometrical analysis and DFT calculations show that the steric bulk of the L-ligand is important, and surprisingly, a large thiolate is not enough to achieve high Z-selectivity. For example, the small trimethylphosphine ligand results in an E-selective catalyst even when combined with the bulky 2,4,6-triphenylbenzenethiolate. With increasing phosphine steric bulk, phosphine–thiolate repulsion will push the thiolate down toward the site of the metallacyclobutane formation and thus induce Z-selectivity.

Lack of phosphine steric bulk allows the thiolate to bend (via the Ru–S–Ar and P–Ru–S angles) upward, toward the phosphine, and, more importantly, to twist around the Ru–S and S–Ar bonds so as to minimize steric repulsion against the metallacyclobutane moiety. Phosphines, in contrast to NHC ligands, are also seen to relax steric repulsion against the thiolate ligand by rotation around the Ru–P bond. A chelating P–O-type ligand prevents this rotation. The most catalytically active and Z-isomer-yielding catalyst obtained here (8b)

contains a bidentate, five-membered-ring-forming *o*-(di-*tert*-butylphosphino)phenolate ligand that prevents rotation, directs bulky *tert*-butyl substituents toward the thiolate, and has little steric hindrance *trans* to the thiolate.

■ COMPUTATIONAL DETAILS

Geometry Optimization. All geometry optimizations were performed using the hybrid range-separated functional including empirical atom–atom dispersion, ω B97XD, as implemented in Gaussian 09.⁵⁸ The ω B97XD^{59–61} functional was chosen due to its excellent performance in reproducing X-ray geometries of ruthenium-based olefin metathesis catalysts and other functional transition metal compounds.⁵² Input geometries were constructed using the Spartan software package⁵² by modifying the available X-ray structures⁶³ or previously DFT-D-optimized geometries and by performing conformational searches at the MMFF⁶⁴ force-field level. The standard procedure consisted of selecting a few of the conformations of lowest MMFF energy for evaluation at the DFT level. The thus obtained conformation with the lowest Gibbs free energy in toluene was used. Tight geometry optimization, corresponding to a maximum force of 1.5×10^{-5} au and the accordingly scaled maximum displacement, was used (keyword opt = (Tight)). Numerical integrations were performed using the “superfine” grid (pruned, 150 radial shells and 974 angular points per shell for the first two rows of the periodic table, 225 shells and 974 angular points per shell for later elements) of Gaussian 09. The SCF density-based convergence criterion was tightened 100-fold compared to the default, to 10^{-10} (keyword SCF = (Conver = 10)). This tightening was necessary to ensure geometry convergence. All stationary points were characterized by the eigenvalues of the analytically calculated Hessian matrix.

The Stuttgart 28-electron relativistic effective core potential (ECP28MDF) in conjunction with the accompanying correlation consistent valence triple- ζ plus polarization (cc-pVTZ-PP) basis set, with the *g* function removed, was used for the Ru atom,⁶⁵ which implies a (41s37p25d2f)/[5s5p4d2f] contraction. The rest of the atoms were treated as follows: All atoms which, at some point in the reaction, are directly bonded (here termed a “nearest neighbor”, via a covalent or donor–acceptor bond) to ruthenium (e.g., the sp^2 carbon atoms of the substrate alkene) were described by correlation consistent valence triple- ζ plus polarization (cc-pVTZ)^{66,67} basis sets, obtained from the EMSL basis set exchange Web site,⁶⁸ in which, in each case, the highest angular momentum functions were removed. Moreover, the same triple- ζ basis sets were used also for the entire sulfonate group in **6** due to highly delocalized electrons and indistinguishable O atoms. The resulting contractions were C, N, O (18s5p2d)/[4s3p2d]; Cl, S (41s16p2d)/[5s4p2d]. All other atoms were described by the standard correlation consistent valence double- ζ plus polarization (cc-pVDZ)^{66,67} basis sets.

Thermochemistry. Translational, rotational, and vibrational partition functions for thermal corrections to give total enthalpies and Gibbs free energies were computed within the ideal-gas, rigid-rotor, and harmonic oscillator approximations following standard procedures, with a minor adjustment for the entropy corrections. To reduce the well-known problems (fluctuations in free energy corrections due to vibrational entropy divergence for low frequencies)^{69,70} caused by the harmonic-approximation low-frequency modes upon calculation of thermochemical corrections,^{69,71–73} we used the quasi-harmonic treatment of Truhlar and co-workers,^{72,73} consisting of shifting all frequencies below 100 cm^{-1} to 100 cm^{-1} , when calculating entropies. The temperature used in the calculation of thermochemical corrections was set to 298.15 K.

Single-Point Calculations (SP). The reported energies were obtained in SP calculations on optimized geometries using the gradient-corrected PBE^{74,75} functional in combination with the D3 version of Grimme’s empirical dispersion with Becke–Johnson damping,⁷⁶ termed PBE-D3(BJ), as implemented in Gaussian 09.⁵⁸ The PBE-D3(BJ) functional was chosen due to its excellent agreement with experimental relative gas-phase energies of ruthenium-mediated olefin metathesis.⁷⁷ Numerical integrations were performed using the

“ultrafine” grid of Gaussian 09. The SP SCF convergence criterion was set to 10^{-5} .

The Stuttgart 28-electron relativistic effective core potential (ECP28MDF) in conjunction with the accompanying correlation consistent valence quadruple- ζ plus polarization (cc-pVQZ-PP) basis set was used for the Ru atom.⁶⁵ The C and H atoms were treated with the correlation consistent valence quadruple- ζ plus polarization (cc-pVQZ)^{66,67} basis sets obtained from the EMSL basis set exchange Web site.⁶⁸ All other atoms were treated with an extended cc-pVQZ basis set obtained by adding diffuse functions from the “aug-cc-pVQZ Diffuse” set,^{67,78} resulting in the following contractions for the modified basis sets: O, N (22s7p4d3f2g)/[6s5p4d3f2g]; Cl, S (43s20p4d3f2g)/[7s6p4d3f2g].

Electrostatic and nonelectrostatic solvent effects were accounted for implicitly using the SMD solvation method, a polarizable continuum model (PCM) that includes alternative cavitation, dispersion, and solute structure reorganization terms and also uses a particular set of atomic radii that modifies the electrostatic contribution compared to regular PCM.⁷⁹ The SMD calculations were performed using Gaussian 09, with default settings.

Free energies were obtained using a standard state corresponding to a 1 M infinitely diluted solution and a temperature of 298.15 K, as $G_{\text{Tot}} = G_{\text{Gas}} + \Delta G_{\text{solvation}} + \Delta G^{1 \text{ atm} \rightarrow 1 \text{ M}}$, where $\Delta G^{1 \text{ atm} \rightarrow 1 \text{ M}} = 1.89 \text{ kcal/mol}$ and accounts for the change in standard state from 1 atm to 1 M.⁷⁷ $\Delta G_{\text{solvation}}$ is the solvation free energy and is the difference between the SMD and the gas-phase SCF energies. G_{gas} is the Gibbs free energy in the gas phase calculated by adding the thermal correction (G_{corr}) to the single-point SCF energy; see the Supporting Information.

■ EXPERIMENTAL SECTION

Reactions were performed under a dry argon atmosphere using Schlenk techniques or in a glovebox, unless otherwise stated. Tetrahydrofuran, toluene, and dichloromethane were dried using an MBraun solvent purification system (“Grubbs column”) and degassed before use. Anhydrous *n*-pentane was purchased from Sigma-Aldrich and used as received. Allyl acetate, allylbenzene, 4-phenyl-1-butene, allyltrimethylsilane, 1-octene, 2-allyloxyethanol, *p*-cymene, and *cis*-cyclooctene were purchased from Sigma-Aldrich and degassed before use. Potassium 2,4,6-trimethylbenzenethiolate,⁴¹ potassium 2,4,6-triphenylbenzenethiolate,⁴² and $[\text{P}(-6\text{-O-C}_6\text{H}_4)(t\text{-Bu})_2]\text{ClRu}(=\text{CH-o-O}^-\text{PrC}_6\text{H}_4)$ ^{49,57} were prepared according to literature procedures. All the other chemicals were purchased from commercial suppliers and used as received.

NMR spectra were recorded on Bruker Biospin AV500 and AV600 spectrometers. The chemical shifts are reported relative to the residual solvent peaks.⁸⁰ Phosphorus resonance spectra were calibrated using a sealed ampule containing 85% aqueous H_3PO_4 , submerged in an NMR tube filled with D_2O , as external standard.⁸¹

HRMS DART and ESI mass spectra were recorded by means of respectively a DART-100 ion source from IonSense Inc. (Saugus, MA, USA) or an orthogonal electron spray ionization ion source (ESI) interfaced to a JMS-T100LC AccuTOF mass spectrometer from JEOL USA, Inc. (Peabody, MA, USA). The ions were transported into the orthogonal accelerating time-of-flight (TOF) single-stage reflectron mass analyzer by a high-frequency and high-voltage quadrupole ion guide. Detection was achieved with a dual microchannel plate detector. Elemental analyses were performed using an Elementar Vario EL III analyzer.

Suitable crystals for diffraction experiments were immersed in Paratone-N (Hampton Research) in a nylon loop. Data collection was done on a Bruker AXS TXS rotating anode system with an APEXII Pt¹³⁵ CCD detector using graphite-monochromated Mo $K\alpha$ radiation ($\lambda = 0.71073 \text{ \AA}$). Data collection and data processing were done using APEX2,⁸² SAINT,⁸³ and SADABS⁸⁴ version 2008/1, or TWINABS,⁸⁵ whereas structure solution and final model refinement were done using SHELXS⁸⁶ version 2013/1 or SHELXT⁸⁷ version 2014/4 and SHELXL⁸⁸ version 2014/7.

[P(Cy)₃](−S-2,4,6-Ph-C₆H₂)ClRu(=CH-o-O[−]PrC₆H₄), **4.** Under an inert atmosphere Hoveyda–Grubbs first-generation catalyst (120.9

mg, 0.20 mmol) and potassium 2,4,6-triphenylbenzenethiolate (80.3 mg, 0.21 mmol) were suspended in 10 mL of THF. After being stirred at room temperature for 24 h most of the solvent was removed *in vacuo*. Dark red crystals of **4** (126 mg, 0.14 mmol, 70%) were grown after addition of *n*-pentane at low temperature ($-32\text{ }^{\circ}\text{C}$). ^1H NMR (500.13 MHz, CD_2Cl_2): δ 14.6 (d, $^3J_{\text{HP}} = 5.3$ Hz, 1H), 7.78–7.64 (m, 2H), 7.62–7.54 (m, 2H), 7.50 (t, $^3J_{\text{HH}} = 7.7$ Hz, 2H), 7.45 (d, $^3J_{\text{HH}} = 2.2$ Hz, 1H), 7.44–7.27 (m, 5H), 7.22 (d, $^3J_{\text{HH}} = 2.3$ Hz, 1H), 7.05–6.72 (m, 8H), 4.74 (sep, $^3J_{\text{HH}} = 6.3$ Hz, 1H), 2.21 (q, $^3J_{\text{HH}} = 11.9$ Hz, 3H), 2.02–1.41 (m, 21H), 1.37 (d, $^3J_{\text{HH}} = 6.3$ Hz, 3H), 1.31–1.11 (m, 9H), 1.08 (d, $^3J_{\text{HH}} = 6.3$ Hz, 3H). $^{13}\text{C}\{^1\text{H}\}$ NMR (125.76 MHz, CD_2Cl_2): δ 252.84, 252.74, 153.43, 148.51, 147.39, 144.38, 144.27, 142.20, 141.60, 141.02, 138.46, 131.18, 129.39, 129.14, 128.63, 128.07, 127.95, 127.57, 127.53, 127.28, 127.12, 126.99, 125.64, 123.79, 122.67, 114.28, 77.33, 36.17, 35.98, 30.46, 29.74, 29.72, 28.51, 28.43, 28.40, 28.32, 26.79, 22.61, 21.32. ^{31}P NMR (202.46 MHz, CD_2Cl_2): δ 58.62. Anal. Calcd (%) for $\text{C}_{52}\text{H}_{62}\text{ClOPRuS}$: C 69.19, H 6.92. Found: C 69.23, H 6.94. HRMS (DART) found (calcd): m/z 900.30661 (900.30851) [$\text{C}_{52}\text{H}_{62}^{35}\text{ClOP}^{102}\text{RuS} + \text{H}$] $^+$.

[P(–6–SO₃–C₆H₄)(Cy)₂]ClRu(=CH–o–OⁱPrC₆H₄), 5. Under an inert atmosphere 2-(dicyclohexylphosphino)benzenesulfonic acid (202.7 mg, 0.571 mmol) and silver carbonate (83.3 mg, 0.302 mmol) were suspended in 20 mL of THF. After 1 h the solution was filtered followed by the addition of Hoveyda–Grubbs first-generation catalyst (123.3 mg, 0.205 mmol), and the mixture was stirred at room temperature for 24 h. The solvent was removed under reduced pressure, and the residue was passed through a silica gel column using *n*-hexane/diethyl ether (1:3) as eluent. Following this, the solvent of the collected brown fraction was removed *in vacuo*, and the product was dissolved in a little THF. Precipitation with *n*-pentane yielded 40 mg (yield = 30%) of complex **5**. ^1H NMR (500.13 MHz, CD_2Cl_2): δ 18.35 (d, $^3J_{\text{HP}} = 6.1$ Hz, 1H), 8.05–8.03 (m, 1H), 7.80–7.58 (m, 5H), 7.26 (d, $^3J_{\text{HH}} = 8.4$ Hz, 1H), 7.20 (t, $^3J_{\text{HH}} = 7.4$ Hz, 1H), 5.42 (sep d, $^3J_{\text{HH}} = 6.4$, 2.1 Hz, 1H), 3.12–3.05 (m, 1H), 2.77–2.69 (m, 1H), 2.37–2.28 (br, 1H), 2.04–1.59 (br, 17H), 1.88 (d, $^3J_{\text{HH}} = 6.3$ Hz, 3H), 1.71 (d, $^3J_{\text{HH}} = 6.4$ Hz, 3H), 1.52–1.09 (m, 8H). $^{13}\text{C}\{^1\text{H}\}$ NMR (125.76 MHz, CD_2Cl_2): δ 305.68, 305.57, 155.66, 155.65, 145.87, 145.80, 132.29, 132.19, 132.15, 132.09, 131.25, 131.24, 128.03, 127.99, 126.65, 126.39, 124.67, 123.51, 114.34, 78.53, 35.30, 35.07, 35.01, 34.79, 30.12, 27.69, 27.61, 27.50, 27.44, 27.41, 27.35, 27.24, 27.16, 27.10, 26.66, 26.15, 26.04, 26.02, 22.08, 21.89. ^{31}P NMR (202.46 MHz, CD_2Cl_2): δ 52.19. Anal. Calcd (%) for $\text{C}_{28}\text{H}_{38}\text{ClO}_4\text{PRuS}$: 0.13 THF–0.13 *n*-pentane: C 53.33, H 6.23. Found: C 53.69, H 6.39. HRMS (ESI $^+$) found (calcd): m/z 661.08644 (661.08581) [$\text{C}_{28}\text{H}_{38}^{35}\text{ClO}_4\text{P}^{102}\text{RuS} + \text{Na}$] $^+$.

[P(–6–SO₃–C₆H₄)(Cy)₂](–S–2,4,6–Ph–C₆H₂)Ru(=CH–o–OⁱPrC₆H₄), 6. In a glovebox, complex **5** [P(–6–SO₃–C₆H₄)(Cy)₂]ClRu(=CH–o–OⁱPrC₆H₄) (64.5 mg, 0.101 mmol) and potassium 2,4,6-triphenylbenzenethiolate (41.3 mg, 0.110 mmol) were suspended in THF (5 mL), and the mixture was stirred at room temperature for 12 h. The dark green solution was filtered, and the solvent removed *in vacuo*. Dark green crystals of **6** (82 mg, 0.0839 mmol, 84%) were grown by layering a solution of the crude product in dichloromethane with *n*-pentane at low temperature ($-32\text{ }^{\circ}\text{C}$). ^1H NMR (600.17 MHz, CD_2Cl_2): δ 15.61 (d, $^3J_{\text{HP}} = 6.0$ Hz, 1H), 7.88–7.84 (m, 1H), 7.82 (br d, $^3J_{\text{HH}} = 7.0$ Hz, 1H), 7.60–7.55 (m, 2H), 7.55–7.43 (m, 7H), 7.40 (tt, $^3J_{\text{HH}} = 7.7$, 1.7 Hz, 2H), 7.35 (br t, $^3J_{\text{HH}} = 6.9$ Hz, 1H), 7.31 (tt, $^3J_{\text{HH}} = 7.3$, 1.3 Hz, 1H), 7.18 (br s, 1H), 7.10 (br t, $^3J_{\text{HH}} = 6.6$ Hz, 1H), 7.05–6.87 (m, 7H), 4.94 (sep, $^3J_{\text{HH}} = 6.6$ Hz, 1H), 2.70–2.57 (m, 2H), 2.56–2.46 (br m, 1H), 2.11–2.01 (br m, 1H), 1.96–1.71 (br m, 7H), 1.67–1.22 (m, 12H), 1.38 (d, $^3J_{\text{HH}} = 6.6$ Hz, 3H), 1.17 (d, $^3J_{\text{HH}} = 6.6$ Hz, 3H), 1.10–0.90 (m, 2H), 0.56–0.43 (m, 1H). $^{13}\text{C}\{^1\text{H}\}$ NMR (150.91 MHz, CD_2Cl_2): δ 275.44, 275.36, 152.97, 149.55, 147.25, 147.19, 147.11, 145.41, 143.77, 141.59, 141.21, 140.98, 138.70, 131.82, 131.27, 130.90, 130.86, 130.75, 129.14, 129.04, 128.61, 128.56, 128.14, 127.87, 127.59, 127.49, 127.08, 126.89, 126.55, 126.33, 125.97, 124.48, 123.08, 115.39, 79.83, 34.33, 34.16, 34.01, 33.83, 28.48, 27.70, 27.62, 27.55, 27.40, 27.35, 27.33, 27.27, 27.11, 27.07, 26.77, 26.49, 26.43, 26.20, 26.18, 21.95, 20.70. ^{31}P NMR (202.46 MHz, CD_2Cl_2): δ 48.68. Anal. Calcd (%) for $\text{C}_{52}\text{H}_{55}\text{O}_4\text{PRuS}_2$: 0.36 *n*-pentane–0.19 THF: C

66.88, H 6.26. Found: C 66.59, H 6.43. HRMS (ESI $^+$) found (calcd): m/z 963.22366 (963.22205) [$\text{C}_{52}\text{H}_{55}\text{O}_4\text{P}^{102}\text{RuS}_2 + \text{Na}$] $^+$.

[P(–6–O–C₆H₄)(^tBu)₂](–S–2,4,6–Me–C₆H₂)Ru(=CH–o–OⁱPrC₆H₄) (8a). In a glovebox [P(–6–O–C₆H₄)(^tBu)₂]ClRu(=CH–o–OⁱPrC₆H₄) (103.2 mg, 0.198 mmol) and potassium 2,4,6-trimethylbenzenethiolate (43.1 mg, 0.226 mmol) were suspended in THF (8 mL), and the mixture was stirred at room temperature for 12 h. The solvent was removed *in vacuo*. The residual was dissolved in *n*-pentane and filtered over Celite. After the solvent was removed *in vacuo* a red powder of **8a** was obtained (116 mg, 0.182 mmol, 92%). ^1H NMR (500.13 MHz, CD_2Cl_2): δ 14.83 (d, $^3J_{\text{HP}} = 5.2$ Hz, 1H), 7.46–7.37 (m, 2H), 7.36–7.31 (m, 1H), 7.05 (ddt, $^3J_{\text{HH}} = 8.4$, 7.0, 1.4 Hz, 1H), 6.98 (dt, $^3J_{\text{HH}} = 7.4$, 1.0 Hz, 1H), 6.89–6.00 (br, 5H), 6.65–6.55 (m, 3H), 4.50 (sep d, $^3J_{\text{HH}} = 6.2$, 1.4 Hz, 1H), 2.96–2.05 (br, 6H), 2.16 (s, 3H), 1.75 (d, $^3J_{\text{HH}} = 13.8$ Hz, 9H), 1.56 (d, $^3J_{\text{HH}} = 13.4$, 9H), 1.42 (s, 1H), 1.30 (m, 8H). $^{13}\text{C}\{^1\text{H}\}$ NMR (125.76 MHz, CD_2Cl_2): δ 245.87, 245.78, 177.55, 177.45, 152.34, 152.33, 144.51, 139.06, 134.38, 132.72, 131.92, 131.91, 127.98, 126.74, 123.34, 122.71, 121.22, 120.91, 118.44, 118.36, 116.07, 116.02, 114.74, 76.43, 40.23, 40.06, 35.10, 34.93, 32.13, 32.11, 30.52, 28.56, 26.74, 21.13, 21.02, 20.99. ^{31}P NMR (202.46 MHz, CD_2Cl_2): δ 93.07. Anal. Calcd (%) for $\text{C}_{33}\text{H}_{45}\text{O}_2\text{PRuS}$: 0.25 *n*-pentane: C 62.72, H 7.38. Found: C 63.14, H 7.09. HRMS (ESI $^+$) found (calcd): m/z 639.20112 (639.19996) [$\text{C}_{33}\text{H}_{45}\text{O}_2\text{P}^{102}\text{RuS} + \text{H}$] $^+$.

[P(–6–O–C₆H₄)(^tBu)₂](–S–2,4,6–Ph–C₆H₂)Ru(=CH–o–OⁱPrC₆H₄) (8b). In a glovebox [P(–6–O–C₆H₄)(^tBu)₂]ClRu(=CH–o–OⁱPrC₆H₄) (108.8 mg, 0.208 mmol) and potassium 2,4,6-triphenylbenzenethiolate (82.3 mg, 0.219 mmol) were suspended in THF (6 mL), and the mixture was stirred at room temperature for 12 h. The solution was filtered, and the solvent removed *in vacuo*. The residual was dissolved in *n*-pentane and filtered. After the solvent was removed *in vacuo* the remaining crude product was dissolved in a minimum amount of dichloromethane. Dark red crystals of **8b** (63 mg, 0.076 mmol, 37%) were grown upon layering the solution with *n*-pentane at low temperature ($-32\text{ }^{\circ}\text{C}$). ^1H NMR (500.13 MHz, CD_2Cl_2): δ 13.97 (d, $^3J_{\text{HP}} = 5.4$, 1H), 7.82–7.76 (m, 2H), 7.62–7.57 (m, 2H), 7.50 (d, $^3J_{\text{HH}} = 2.2$ Hz, 1H), 7.47–7.37 (m, 4H), 7.37–7.27 (m, 3H), 7.25–7.16 (m, 2H), 7.09–7.04 (m, 2H), 7.01 (tt, $^3J_{\text{HH}} = 7.4$, 1.2 Hz, 1H), 6.94–6.87 (m, 2H), 6.87–6.75 (m, 4H), 6.47–6.41 (m, 1H), 6.41–6.34 (m, 1H), 4.71 (sep d, $^3J_{\text{HH}} = 6.2$, 0.7 Hz, 1H), 1.59 (d, $^3J_{\text{HH}} = 13.8$ Hz, 9H), 1.38 (d, $^3J_{\text{HH}} = 6.2$ Hz, 3H), 1.18 (br d, $^3J_{\text{HH}} = 12.1$ Hz, 9H), 0.98 (d, $^3J_{\text{HH}} = 6.2$ Hz, 3H). $^{13}\text{C}\{^1\text{H}\}$ NMR (125.76 MHz, CD_2Cl_2): δ 247.95, 247.84, 177.43, 177.33, 153.46, 153.45, 148.95, 147.47, 144.44, 143.80, 143.63, 141.60, 141.29, 138.11, 132.69, 131.63, 131.50, 129.13, 128.78, 127.83, 127.49, 127.45, 127.25, 127.15, 126.71, 126.69, 125.74, 123.25, 122.93, 121.04, 120.73, 118.17, 118.10, 115.64, 115.59, 113.27, 76.87, 40.13, 39.96, 35.09, 34.93, 31.90, 31.88, 28.15, 21.87, 20.67. ^{31}P NMR (202.46 MHz, CD_2Cl_2): δ 90.25. Anal. Calcd (%) for $\text{C}_{48}\text{H}_{51}\text{O}_2\text{PRuS}$: 0.2 *n*-pentane–0.6 DCM: C 66.98, H 6.19. Found: C 66.71, H 5.96. HRMS (ESI $^+$) found (calcd): m/z 824.24873 (824.24814) [$\text{C}_{48}\text{H}_{51}\text{O}_2\text{P}^{101}\text{RuS} + \text{H}$] $^+$.

■ ASSOCIATED CONTENT

Supporting Information

The Supporting Information is available free of charge on the ACS Publications website at DOI: 10.1021/acs.organomet.6b00214.

Spectral (^1H , ^{13}C , and ^{31}P NMR) and X-ray refinement data for new compounds, calculated electronic energies and thermochemical and solvent corrections, and sample input files (PDF)

Computed molecular Cartesian coordinates in a format convenient for visualization (XYZ)

X-ray crystallographic data for **4** (CCDC-1458097) (CIF)

X-ray crystallographic data for **6** (CCDC-1458098) (CIF)

X-ray crystallographic data for **8b** (CCDC-1458099) (CIF)

AUTHOR INFORMATION

Corresponding Authors

*E-mail: Giovanni.Occhipinti@uib.no.

*E-mail: Vidar.Jensen@uib.no.

Notes

The authors declare no competing financial interest.

ACKNOWLEDGMENTS

The authors gratefully acknowledge the Research Council of Norway for financial support via the FORNY2020 (grant number 203379 and 239288) and GASSMAKS (208335) programs and for CPU and storage resources granted through the NOTUR (NN2506K) and NORSTORE (NS2506K) supercomputing programs. W.S. acknowledges the University of Bergen for a doctoral fellowship. Dr. Bjarte Holmelid is thanked for assistance with the HRMS (DART and ESI⁺) analyses.

REFERENCES

- Hog, D. T.; Huber, F. M. E.; Mayer, P.; Trauner, D. *Angew. Chem., Int. Ed.* **2014**, *53*, 8513–8517.
- Seetharamsingh, B.; Rajamohanam, P. R.; Reddy, D. S. *Org. Lett.* **2015**, *17*, 1652–1655.
- Sulake, R. S.; Chen, C. *Org. Lett.* **2015**, *17*, 1138–1141.
- Elacqua, E.; Weck, M. *Chem. - Eur. J.* **2015**, *21*, 7151–7158.
- Martinez, H.; Ren, N.; Matta, M. E.; Hillmyer, M. A. *Polym. Chem.* **2014**, *5*, 3507–3532.
- Rybak, A.; Fokou, P. A.; Meier, M. A. R. *Eur. J. Lipid Sci. Technol.* **2008**, *110*, 797–804.
- Kim, Y.-W.; Grossmann, T. N.; Verdine, G. L. *Nat. Protoc.* **2011**, *6*, 761–771.
- Walensky, L. D.; Bird, G. H. *J. Med. Chem.* **2014**, *57*, 6275–6288.
- Chhabra, S.; Belgi, A.; Bartels, P.; van Lierop, B. J.; Robinson, S. D.; Kompella, S. N.; Hung, A.; Callaghan, B. P.; Adams, D. J.; Robinson, A. J.; Norton, R. S. *J. Med. Chem.* **2014**, *57*, 9933–9944.
- Lin, Y. A.; Chalker, J. M.; Davis, B. G. *ChemBioChem* **2009**, *10*, 959–969.
- Mangold, S. L.; O'Leary, D. J.; Grubbs, R. H. *J. Am. Chem. Soc.* **2014**, *136*, 12469–12478.
- Feuillastre, S.; Piva, O. *Synlett* **2014**, *25*, 2883–2886.
- Yu, M.; Wang, C.; Kyle, A. F.; Jakubec, P.; Dixon, D. J.; Schrock, R. R.; Hoveyda, A. H. *Nature* **2011**, *479*, 88–93.
- Flook, M. M.; Jiang, A. J.; Schrock, R. R.; Müller, P.; Hoveyda, A. H. *J. Am. Chem. Soc.* **2009**, *131*, 7962–7963.
- Jiang, A. J.; Zhao, Y.; Schrock, R. R.; Hoveyda, A. H. *J. Am. Chem. Soc.* **2009**, *131*, 16630–16631.
- Marinescu, S. C.; Schrock, R. R.; Müller, P.; Takase, M. K.; Hoveyda, A. H. *Organometallics* **2011**, *30*, 1780–1782.
- Keitz, B. K.; Endo, K.; Herbert, M. B.; Grubbs, R. H. *J. Am. Chem. Soc.* **2011**, *133*, 9686–9688.
- Keitz, B. K.; Endo, K.; Patel, P. R.; Herbert, M. B.; Grubbs, R. H. *J. Am. Chem. Soc.* **2012**, *134*, 693–699.
- Endo, K.; Grubbs, R. H. *J. Am. Chem. Soc.* **2011**, *133*, 8525–8527.
- Khan, R. K. M.; Torker, S.; Hoveyda, A. H. *J. Am. Chem. Soc.* **2013**, *135*, 10258–10261.
- Khan, R. K. M.; Torker, S.; Hoveyda, A. H. *J. Am. Chem. Soc.* **2014**, *136*, 14337–14340.
- Koh, M. J.; Khan, R. K. M.; Torker, S.; Hoveyda, A. H. *Angew. Chem., Int. Ed.* **2014**, *53*, 1968–1972.
- Vyboishchikov, S. F.; Bühl, M.; Thiel, W. *Chem. - Eur. J.* **2002**, *8*, 3962–3975.
- Adlhart, C.; Chen, P. *J. Am. Chem. Soc.* **2004**, *126*, 3496–3510.
- Ashworth, I. W.; Hillier, I. H.; Nelson, D. J.; Percy, J. M.; Vincent, M. A. *ACS Catal.* **2013**, *3*, 1929–1939.
- Benitez, D.; Tkatchouk, E.; Goddard, W. A., III. *Chem. Commun.* **2008**, 6194–6196.
- Cavallo, L. *J. Am. Chem. Soc.* **2002**, *124*, 8965–8973.
- Fomine, S.; Vargas, S. M.; Tlenkopatchev, M. A. *Organometallics* **2003**, *22*, 93–99.
- Lippstreu, J. J.; Straub, B. F. *J. Am. Chem. Soc.* **2005**, *127*, 7444–7457.
- Nunez-Zarur, F.; Solans-Monfort, X.; Rodriguez-Santiago, L.; Pleixats, R.; Sodupe, M. *Chem. - Eur. J.* **2011**, *17*, 7506–7520.
- Nunez-Zarur, F.; Solans-Monfort, X.; Rodriguez-Santiago, L.; Sodupe, M. *Organometallics* **2012**, *31*, 4203–4215.
- Piacenza, M.; Hyla-Kryspin, I.; Grimme, S. *J. Comput. Chem.* **2007**, *28*, 2275–2285.
- Webster, C. E. *J. Am. Chem. Soc.* **2007**, *129*, 7490–7491.
- Romero, P. E.; Piers, W. E. *J. Am. Chem. Soc.* **2005**, *127*, 5032–5033.
- Romero, P. E.; Piers, W. E. *J. Am. Chem. Soc.* **2007**, *129*, 1698–1704.
- van der Eide, E. F.; Romero, P. E.; Piers, W. E. *J. Am. Chem. Soc.* **2008**, *130*, 4485–4491.
- Wenzel, A. G.; Grubbs, R. H. *J. Am. Chem. Soc.* **2006**, *128*, 16048–16049.
- Jensen, V. R.; Occhipinti, G.; Hansen, F. R. *Novel Olefin Metathesis Catalysts*. Patent WO2012032131, 2012.
- Nelson, J. W.; Grundy, L. M.; Dang, Y.; Wang, Z.-X.; Wang, X. *Organometallics* **2014**, *33*, 4290–4294.
- Liu, P.; Xu, X.; Dong, X.; Keitz, B. K.; Herbert, M. B.; Grubbs, R. H.; Houk, K. N. *J. Am. Chem. Soc.* **2012**, *134*, 1464–1467.
- Occhipinti, G.; Hansen, F. R.; Törnroos, K. W.; Jensen, V. R. *J. Am. Chem. Soc.* **2013**, *135*, 3331–3334.
- Occhipinti, G.; Koudriavtsev, V.; Törnroos, K. W.; Jensen, V. R. *Dalton Trans.* **2014**, *43*, 11106–11117.
- Gimeno, N.; Formentin, P.; Steinke, J. H. G.; Vilar, R. *Eur. J. Org. Chem.* **2007**, *2007*, 918–924.
- Occhipinti, G.; Bjørsvik, H. R.; Jensen, V. R. *J. Am. Chem. Soc.* **2006**, *128*, 6952–6964.
- Trnka, T. M.; Grubbs, R. H. *Acc. Chem. Res.* **2001**, *34*, 18–29.
- Higman, C. S.; Plais, L.; Fogg, D. E. *ChemCatChem* **2013**, *5*, 3548–3551.
- Lee, C. W.; Grubbs, R. H. *Org. Lett.* **2000**, *2*, 2145–2147.
- Bornand, M.; Torker, S.; Chen, P. *Organometallics* **2007**, *26*, 3585–3596.
- Torker, S.; Muller, A.; Sigrist, R.; Chen, P. *Organometallics* **2010**, *29*, 2735–2751.
- Jovic, M. *Structure - Reactivity Relationships in Novel Ruthenium and Rhenium Olefin Metathesis Catalysts*. Ph.D. Thesis, ETH Zurich, Zurich, 2014.
- Heisterberg, D. J. *The Quatfit Program*; The CCL Archive, 1990.
- Minenkov, Y.; Singstad, Å.; Occhipinti, G.; Jensen, V. R. *Dalton Trans.* **2012**, *41*, 5526–5541.
- Bashir, O.; Piche, L.; Claverie, J. P. *Organometallics* **2014**, *33*, 3695–3701.
- Occhipinti, G.; Bjørsvik, H.-R.; Törnroos, K. W.; Jensen, V. R. *Organometallics* **2007**, *26*, 5803–5814.
- Thiel, V.; Hendann, M.; Wännowius, K.-J.; Plenio, H. *J. Am. Chem. Soc.* **2012**, *134*, 1104–1114.
- Rauchfuss, T. B. *Inorg. Chem.* **1977**, *16*, 2966–2968.
- Torker, S.; Mueller, A.; Chen, P. *Angew. Chem., Int. Ed.* **2010**, *49*, S3762/1–S3762/47.
- Frisch, M. J.; Trucks, G. W.; Schlegel, H. B.; Scuseria, G. E.; Robb, M. A.; Cheeseman, J. R.; Scalmani, G.; Barone, V.; Mennucci, B.; Petersson, G. A.; Nakatsuji, H.; Caricato, M.; Li, X.; Hratchian, H. P.; Izmaylov, A. F.; Bloino, J.; Zheng, G.; Sonnenberg, J. L.; Hada, M.; Ehara, M.; Toyota, K.; Fukuda, R.; Hasegawa, J.; Ishida, M.; Nakajima, T.; Honda, Y.; Kitao, O.; Nakai, H.; Vreven, T.; Montgomery, J. A., Jr.; Peralta, J. E.; Ogliaro, F.; Bearpark, M.; Heyd, J. J.; Brothers, E.; Kudin, K. N.; Staroverov, V. N.; Keith, T.; Kobayashi, R.; Normand, J.;

Raghavachari, K.; Rendell, A.; Burant, J. C.; Iyengar, S. S.; Tomasi, J.; Cossi, M.; Rega, N.; Millam, J. M.; Klene, M.; Knox, J. E.; Cross, J. B.; Bakken, V.; Adamo, C.; Jaramillo, J.; Gomperts, R.; Stratmann, R. E.; Yazyev, O.; Austin, A. J.; Cammi, R.; Pomelli, C.; Ochterski, J. W.; Martin, R. L.; Morokuma, K.; Zakrzewski, V. G.; Voth, G. A.; Salvador, P.; Dannenberg, J. J.; Dapprich, S.; Daniels, A. D.; Farkas, Ö.; Foresman, J. B.; Ortiz, J. V.; Cioslowski, J.; Fox, D. J. *Gaussian 09*, Revision D.01; Gaussian, Inc.: Wallingford, CT, 2013.

- (59) Becke, A. D. *J. Chem. Phys.* **1997**, *107*, 8554–8560.
- (60) Chai, J. D.; Head-Gordon, M. *Phys. Chem. Chem. Phys.* **2008**, *10*, 6615–6620.
- (61) Wu, Q.; Yang, W. T. *J. Chem. Phys.* **2002**, *116*, 515–524.
- (62) *Spartan '08*; Wavefunction, Inc.: Irvine, CA, 2008.
- (63) Allen, F. H. *Acta Crystallogr., Sect. B: Struct. Sci.* **2002**, *58*, 380–388.
- (64) Halgren, T. A. *J. Comput. Chem.* **1996**, *17*, 490–519.
- (65) Peterson, K. A.; Figgen, D.; Dolg, M.; Stoll, H. *J. Chem. Phys.* **2007**, *126*, 126.
- (66) Dunning, T. H. *J. Chem. Phys.* **1989**, *90*, 1007–1023.
- (67) Woon, D. E.; Dunning, T. H. *J. Chem. Phys.* **1993**, *98*, 1358–1371.
- (68) Feller, D. *J. Comput. Chem.* **1996**, *17*, 1571–1586.
- (69) Grimme, S. *Chem. - Eur. J.* **2012**, *18*, 9955–9964.
- (70) Scott, A. P.; Radom, L. *J. Phys. Chem.* **1996**, *100*, 16502–16513.
- (71) Katzer, G.; Sax, A. F. *J. Comput. Chem.* **2005**, *26*, 1438–1451.
- (72) Zhao, Y.; Truhlar, D. G. *Phys. Chem. Chem. Phys.* **2008**, *10*, 2813–2818.
- (73) Ribeiro, R. F.; Marenich, A. V.; Cramer, C. J.; Truhlar, D. G. *J. Phys. Chem. B* **2011**, *115*, 14556–14562.
- (74) Perdew, J. P.; Burke, K.; Ernzerhof, M. *Phys. Rev. Lett.* **1996**, *77*, 3865–3868.
- (75) Perdew, J. P.; Burke, K.; Ernzerhof, M. *Phys. Rev. Lett.* **1997**, *78*, 1396–1396.
- (76) Grimme, S.; Ehrlich, S.; Goerigk, L. *J. Comput. Chem.* **2011**, *32*, 1456–1465.
- (77) Minenkov, Y.; Occhipinti, G.; Jensen, V. R. *Organometallics* **2013**, *32*, 2099–2111.
- (78) Kendall, R. A.; Dunning, T. H.; Harrison, R. J. *J. Chem. Phys.* **1992**, *96*, 6796–6806.
- (79) Marenich, A. V.; Cramer, C. J.; Truhlar, D. G. *J. Phys. Chem. B* **2009**, *113*, 6378–6396.
- (80) Fulmer, G. R.; Miller, A. J. M.; Sherden, N. H.; Gottlieb, H. E.; Nudelman, A.; Stoltz, B. M.; Bercaw, J. E.; Goldberg, K. I. *Organometallics* **2010**, *29*, 2176–2179.
- (81) Kühn, O. *Phosphorus-31 NMR Spectroscopy*. Springer-Verlag: Heidelberg, 2008.
- (82) *APEX2*, Version 2014.11-0; Bruker-AXS: Madison, WI, USA, 2014.
- (83) *SAINT*, Version 7.68A; Bruker-AXS: Madison, WI, USA, 2010.
- (84) Krause, L.; Herbst-Irmer, R.; Sheldrick, G. M.; Stalke, D. *J. Appl. Crystallogr.* **2015**, *48*, 3–10.
- (85) Sheldrick, G. M. *TWINABS*, Version 2012/1; Georg-August-Universität Göttingen: Göttingen, Germany, 2012.
- (86) Sheldrick, G. M. *XS*, Version 2013/1; Georg-August-Universität Göttingen: Göttingen, Germany, 2013.
- (87) Sheldrick, G. *Acta Crystallogr., Sect. A: Found. Adv.* **2015**, *71*, 3–8.
- (88) Sheldrick, G. *Acta Crystallogr., Sect. C: Struct. Chem.* **2015**, *71*, 3–8.